JACS
JOURNAL OF THE AMERICAN CHEMICAL SOCIETY
Article
pubs.acs.org/JACS

Ternary Gold Hydrides: Routes to Stable and Potentially Superconducting Compounds

Martin Rahm,*[,†,§] Roald Hoffmann,*[,†] and N. W. Ashcroft[‡]

[†]Department of Chemistry and Chemical Biology and [‡]Laboratory of Atomic and Solid State Physics, Cornell University Ithaca, New York 14853, United States

Supporting Information

ABSTRACT: In a search for gold hydrides, an initial discouraging result of no theoretical stability in any binary AuH_n at $P < 300$ GPa was overcome by introducing alkali atoms as reductants. A set of $AAuH_2$ compounds, A = Li, Na, K, Rb, and Cs, is examined; of these, certain K, Rb, and Cs compounds are predicted to be thermodynamically stable. All contain AuH_2^- molecular units and are semiconducting at $P = 1$ atm, and some form metallic and superconducting symmetrically bonded AuHAu sheets under compression. To induce metallicity by bringing the Au atoms closer together under ambient conditions, we examined alkaline earth ion substitution for two A, i.e., materials of composition $AE(AuH_2)_2$. For AE = Ba and Sr, the materials are already marginally metallic at $P = 1$ atm and the combination of high and low phonon frequencies and good electron−phonon coupling leads to reasonably high calculated superconducting transition temperatures for these materials.

INTRODUCTION

Our aim in this work is to pursue a realistic route to gold hydrides in the condensed state. The challenge we face is that gold is one of the least reactive metals. Gold, along with a few other noble metals, resists surface oxidation under ambient conditions. Whereas some gold alloys with alkali metals, transition metals, and compounds with main group elements, such as halides, exist, one way that gold's inert nature is reflected is by the absence of stable hydrides in the condensed state. This is in sharp contrast to most other metals, which readily form binary alloys, or interstitial or molecular compounds with hydrogen. The passivity of gold can be expressed in still another way—almost every molecular anion will reduce gold ions (Au^+ and Au^{3+}) to pure gold. Or, alternatively, there are few gold compounds with negative formation energies.

An additional motivation for pursuing metal hydride systems in general, and gold hydrides in particular, is that the combination of high phonon frequencies associated with hydrogen and low ones for the heavy gold motions are two factors suggestive of potential high temperature superconductivity in compounds of these elements.[1−3]

The literature reports attempts to fabricate gold hydrides, but high-pressure experiments attempting the synthesis of gold hydrides up to 113 GPa have so far failed.[4] However, inelastic neutron scattering has provided evidence for the existence of surface gold hydride on nanostructured gold catalysts.[5] Different theoretically plausible solid-state structures of AuH have also been discussed.[6]

While relatively scarce, both molecular and extended gold compounds, with negative heats of formation, do exist. Examples include gold halides (both molecular and extended), alkali gold binaries (which we will discuss later on), and alkali gold oxide ternaries.[7−9] Metastable gold species, such as Au_2O_3, have also been made.[10−12] One of us participated in a study of AuO at various pressures that is relevant here.[13] Gold hydrides have been detected as fleeting molecular gas-phase species,[14] and as the products of laser-ablation in low temperature Ar and Ne matrices.[15,16] Gold surfaces and variously sized gold clusters and complexes have, somewhat surprisingly, proven active as catalysts.[17−19] The reasons behind the observed catalytic activity have been discussed at some length.[20] A variety of molecular gold-hydride complexes (Au−H containing molecules) have been made.[21,22] Among these, we mention, by way of example, N-heterocyclic carbene stabilized gold(I) monohydride,[23] dinuclear gold(I) hydrides stabilized by chelating phosphorus-containing ligands,[24] and gold(III) monohydride stabilized by C−N−C pincer ligands.[25,26] Gold's interactions with hydrogen (within molecules) have been thoroughly reviewed.[27] One molecular example is shown in Figure 1.

RESULTS AND DISCUSSION

Are Binary Gold Hydrides Feasible? Whereas we will, as the title of this work suggests, provide what we believe to be a realistic route to gold hydrides at $P = 1$ atm, we first explored high-pressure conditions. The pressure variable can create new chemistries.[28,29] Given the experimental evidence against the existence of gold hydride in the solid state both at 1 atm and under pressure up to 113 GPa,[4] we first investigated whether the application of pressures beyond 100 GPa might change the situation. Unfortunately, particle-swarm optimization structure

Received: May 1, 2017
Published: June 19, 2017

DOI: 10.1021/jacs.7b04456
J. Am. Chem. Soc. 2017, 139, 8740−8751

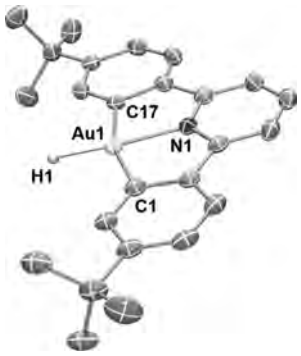

Figure 1. Molecular structure of a "pincer complex" [(C^N^C)*AuH] in the solid state. Hydrogen atoms (except for that bound to the gold atom) are omitted. The hydrogen atom attached to the gold center was located in the electron density map. Selected bond distances and angles (Å and deg): Au−N1, 2.035(3); Au−C17, 2.073(4); Au−C1, 2.074(4); C17−Au−C1, 161.63(16). Reproduced with permission from ref 25.

searches at 100 and 200 GPa on the binaries AuH_2, AuH, Au_3H_2, Au_2H_1, Au_3H, Au_4H, and Au_5H, and subsequent pressure scans up to 300 GPa, showed no evidence for a pressure-induced negative heat of formation for any hydride (Figure 2). We limited our search to pressures below 300 GPa,

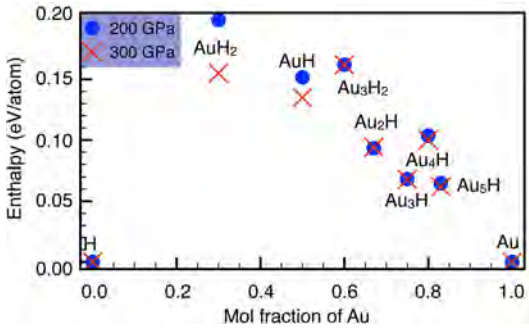

Figure 2. High pressure (≤300 GPa) cannot be used to synthesize binary gold hydrides. The enthalpy of formation (all positive) per atom is plotted at several pressures. Blue dots and red crosses denote the phases calculated to be the least unstable with respect to decomposition into H_2(s) and Au(s) at a given stoichiometry, at 200 and 300 GPa, respectively.

because of a known phase transition in pure gold at ∼290 GPa. So we cannot exclude the possibility that even higher pressures could lead to a AuH binary phase that is thermodynamically favorable relative to the elements.

Many of the low-energy binary Au_xH_y structures identified were of low symmetry, and most were close to degenerate in energy with other structures. This is likely a consequence of the search algorithms proceeding toward the enthalpically most favored state, which appears to be phase separation into elemental gold and hydrogen (this was implied by some of the optimized structures). Metastable structures without a clear route to synthesis, and with likely low barriers of activation to thermal decomposition, are of little practical interest. We have therefore not analyzed these binaries in detail, but selected structures are provided in the Supporting Information (SI). We now return to atmospheric conditions, and a different strategy for stabilizing gold hydrides.

How to Stabilize Gold Hydrides. The unfavorable formation of extended AuH (or other stochiometries) might be traced to the similar electronegativity of hydrogen and gold (Au = 2.54, H = 2.2 on the Pauling scale, and Au = 1.92, H = 2.3 on the Allen scale),[30,31] which militates against Au → H (or Au ← H) charge transfer necessary for ionic lattice stabilization. With the pressure option exhausted, we must perturb this balance in other ways, by the explicit introduction of additional electrons (or holes). Promising clues comes from gold's neighbors in the periodic table, and from extended structures of group 10 and 12 compounds containing MH_2 molecular units.

Consider, for instance, the transfer of one electron from an alkali metal atom to a gold atom. The electron affinity of gold is high. The resulting auride anion, Au^-, is considerably less electronegative than Au, and will interact differently with hydrogen. Specifically, Au^- will allow for Au → H charge transfer to occur. Au^- has a $d^{10}s^2$ electronic configuration, and is, as such, iso-valence-electronic with Zn, Cd, and Hg, which form ZnH_2, CdH_2, and HgH_2 as molecular metastable solids.[32,33] In the latter, the H is formally hydridic and the metals take up a +2 oxidation state. The isoelectronic bonding analogy is with AuH_2^-, a formally d^{10} ML_2 complex featuring Au(I) that is expected to be linear.

Pd^{2-} and Pt^{2-} are also iso-valence-electronic with Au^-, and form linear PdH_2^{2-} and PtH_2^{2-} ions, readily stabilized in the solid state as persistent $[A]_2PdH_2$ and $[A]_2PtH_2$ salts (A = alkali metal).[34−39] Several of these molecular solids show a surprising metallicity, which has been explained as arising from alkali metal s-states crossing the Fermi level.[40−42] Pursued for possible hydrogen storage[43,44] and high temperature applications, their design and synthesis is an active field of research.[45,46]

Auride salts can be readily generated in the presence of strong reducing agents, such as alkali metals. Several different kinds of alkali metal gold binaries are known.[47−54] They exhibit a range of properties, from, for instance, metallic KAu, to semiconducting RbAu and CsAu, with the latter having a band gap of ∼2.6 eV.[55] So, could such compounds be made to react with hydrogen, and is it possible then to stabilize AuH_2^- salts in the solid state?

The AuH_2^- Anion. The AuH_2^- anion has been detected spectroscopically in matrix isolation experiments, using isotope labeling.[56] We know, from high-level multiconfigurational calculations,[57] that AuH_2^- in isolation has a significant barrier to decomposition, a process which eventually proceeds through bond dissociation to Au^- and H_2. The large barrier, which amounts to 57 kcal/mol (2.5 eV) in vacuum, is likely reduced somewhat in an extended system, when the AuH_2^- anion is surrounded by counterions that might facilitate Au^- formation. However, it appears clear that, from a kinetic point of view, a AuH_2^-−based salt might be persistent enough for room temperature handling. Whether such a material will be thermodynamically stable with respect to potential reagents and decomposition products is an entirely different question, however. And one we will attempt to settle.

TERNARY ALKALI METAL GOLD HYDRIDE, $[A]AuH_2$

Extensive structure searches using a particle swarm optimization algorithm (see the Methodology section) were performed on $[A]AuH_2$ stoichiometries (here A = Li, Na, K, Rb, Cs), while allowing for 1−4 formula units in each unit cell. Different

DOI: 10.1021/jacs.7b04456
J. Am. Chem. Soc. 2017, 139, 8740−8751

dynamically stable phases were identified, some by the search algorithm directly, and some by following imaginary phonon modes out of some of the structures found by the search algorithm. The lowest energy phases of each alkali salt were then also recomputed for the other alkali metal counterions, to effectively increase the search space. Several phases were found close in energy, and all of these contain separate AuH_2^- anions, as expected. The lowest energy structure identified for all alkali metals is of $C2$ symmetry (Figure 3).

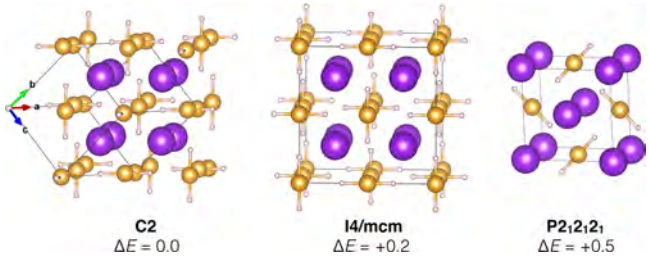

Figure 3. Predicted $C2$ ground state of $KAuH_2$ (1 atm), and two dynamically stable higher energy phases. Relative energies are given in kcal/mol formula unit.

The [A]AuH_2 ($C2$) ground state can be understood in another way as a formal hydrogenation product of gold, forming AuH_2^-, inside of a CsCl-type AAu ($Pm\bar{3}m$) sublattice (Figure 4). The linear AuH_2^- anions can orient themselves in

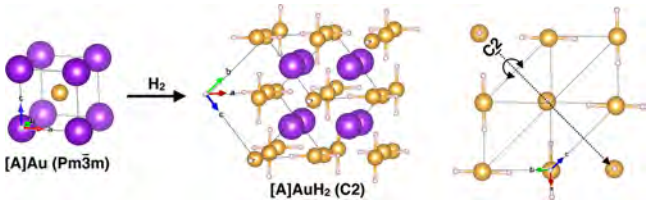

Figure 4. Left: The predicted $C2$ ground state of [A]AuH_2 can be understood as a formal hydrogenation of [A]Au (A = alkali metal). Right: The AuH_2 anionic sublattice in [A]AuH_2 ($C2$) can be viewed as a 2D-plane that repeats also in the third dimension. Arrows indicate the twofold rotational symmetry of the lattice.

different ways in the AAu sublattice, generating several stable or metastable configurations close in energy over a range of pressures. Compare, for instance, the $C2$ and $I4/mcm$ phases in Figure 3. The $C2$ ground state minimizes Au−Au and maximizes AuH−Au distances in a manner symmetric in all three dimensions, as shown in Figure 4.

Thermodynamic Stability. To evaluate the thermodynamic stability of the target alkali metal gold hydrides one must, ideally, know the relative Gibbs energy of all possible decomposition products. The exploration of the complete isomer space of a ternary stoichiometry is a substantial challenge. It reduces to knowing all stable binary compositions, located on the edges of the triangle in Figure 5. Fortunately, our case is simplified by the absence of stable binary gold hydrides (Figure 1), and the prevalence of only one stable (ionic) A_1H_1 binary stoichiometry, at least under ambient conditions,[58−61] which is our focus here. What remains to be determined is a knowledge of stable compositions of the gold alkali metal binaries. And there are several of these. For $KAuH_2$ we have considered 5 compositions, KAu_5, KAu_2, K_2Au_3, KAu,

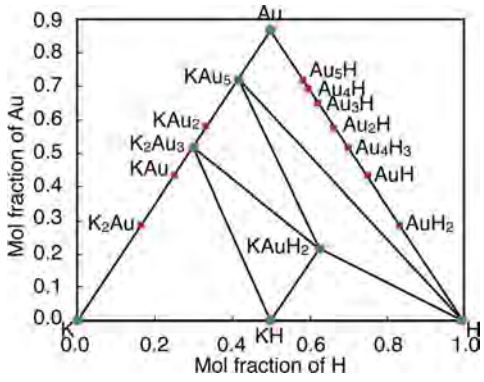

Figure 5. Calculated three-component phase diagram of K, Au, and H as $T \rightarrow 0$ K. Red squares denote unstable compositions (above the convex hull). Black lines between green circles connect stable phases. $KAuH_2$ is predicted to be stable with respect to decomposition into all binaries considered here.

and K_2Au, experimentally known to be stable on the convex hulls of one (or another) alkali metal auride.[62]

All alkali metal gold hydrides exhibit negative energies of formation relative to the elements (Table 1). This, however, is *not* a guarantee of actual thermodynamic stability. $LiAuH_2$ is, for example, unstable with respect to the formation of LiH, Au_3Li and H_2. $NaAuH_2$ is similarly unstable with respect to NaH, $NaAu_2$ and H_2. The lightest compound for which we can expect thermodynamic stability under ambient conditions appears to be $KAuH_2$. Phonon calculations have allowed extrapolation of thermal and entropic corrections to the electronic energy. Even considering the considerable entropic gain associated with gaseous H_2 formation, $KAuH_2$ is predicted to remain stable at room temperature. The margin of stability in Gibbs energy is small, however, only 0.7 kcal/mol, which is below the accuracy of our methodology. More certain appears the thermodynamic stability of $RbAuH_2$ and $CsAuH_2$ (Table 1), the latter being the best candidate for synthesis.

Table 1 shows ΔE and selected ΔH and ΔG both at 300 K for some formation routes of $AAuH_2$. The table is complex to view, but then so is the thermodynamic richness of any ternary compound.

What structures are $AAuH_2$ (A = K, Rb, and Cs) likely to have? Structure searches did not always identify the $C2$ ground state as lowest in energy for those compounds, but when independently refined this structure was consistently lowest in energy. Whether it is in fact the true ground state structure, future experimental work and X-ray spectroscopy will hopefully reveal. Our main conclusion remains that the K^+, Rb^+, and Cs^+ salts of AuH_2^- are thermodynamically accessible, and stable at $P = 1$ atm. If another lower energy crystal structure exists, it will only make this conclusion more certain.

To validate the relative accuracy of our electronic ground state ($T \rightarrow 0$ K) energies shown in Table 1, we performed PBE and HSE06 calculations on the least favorable formation reaction: $1/3K_2Au_3(s) + 1/3KH(s) + 5/6H_2(g) \rightarrow KAuH_2$. We here considered the $P2_12_12_1$ metastable phase of $KAuH_2$, which has a much smaller unit cell compared to the $C2$ ground state. The reaction energy calculates as −7.4 and −9.0 kcal/mol with PBE and HSE06, respectively. This agreement implies that PBE slightly underestimates the stability of the alkali gold metal hydrides, and suggests that our overall PBE-based stability estimates are conservative.

DOI: 10.1021/jacs.7b04456
J. Am. Chem. Soc. 2017, 139, 8740−8751

Table 1. Selection of Formation Routes to Alkali Metal (A= Li, Na, K, Rb, and Cs) Gold Hydrides[a]

	ΔE	ΔE + ZPE	ΔH_{300K}	ΔG_{300K}
$Li(s) + Au(s) + H_2(g) \rightarrow LiAuH_2$	−16.2	–	–	–
$LiH(s) + Au(s) + {}^1/_2H_2(g) \rightarrow LiAuH_2$	+3.1	–	–	–
$ {}^1/_3Li_3Au(s) + {}^2/_3Au(g) + H_2(g) \rightarrow LiAuH_2$	+3.2	–	–	–
$ {}^2/_3LiH(s) + {}^1/_3Au_3Li(s) + {}^2/_3H_2(g) \rightarrow LiAuH_2$	+8.3	–	–	–
$Na(s) + Au(s) + H_2(g) \rightarrow NaAuH_2$	−17.3	–	–	–
$ {}^1/_2NaH(s) + {}^1/_2NaAu_2 + {}^3/_4H_2 \rightarrow NaAuH_2$	+0.6	–	–	–
$ {}^1/_2Na_2Au(s) + {}^1/_2Au + H_2 \rightarrow NaAuH_2$	+7.6	–	–	–
$K(s) + Au(s) + H_2(g) \rightarrow KAuH_2$	−22.9	−20.7	−22.2	−13.8
$ {}^1/_2K_2Au(s)$[b] $ + {}^1/_2Au + H_2 \rightarrow KAuH_2$	−16.8	–	–	–
$Au(s) + KH(s) + {}^1/_2H_2(g) \rightarrow KAuH_2$	−14.9	−12.2	−12.9	−9.8
$KAu(s) + H_2(g) \rightarrow KAuH_2$	−10.6	−8.3	−9.9	−1.1
$ {}^1/_5KAu_5 + {}^4/_5KH + {}^3/_5H_2 \rightarrow KAuH_2$	−10.1	–	–	–
$ {}^1/_2KAu_2 + {}^1/_2KH + {}^3/_4H_2 \rightarrow KAuH_2$	−9.0	–	–	–
$ {}^1/_3K_2Au_3(s) + {}^1/_3KH(s) + {}^5/_6H_2(g) \rightarrow KAuH_2$	−7.8	−5.6	−6.7	−0.7
$Rb(s) + Au(s) + H_2(g) \rightarrow RbAuH_2$	−23.8	–	–	–
$RbAu(s) + H_2(g) \rightarrow RbAuH_2$	−10.7	–	–	–
$ {}^1/_3Rb_2Au_3(s) + {}^1/_3RbH(s) + {}^5/_6H_2(g) \rightarrow RbAuH_2$	−9.6	–	–	–
$Cs(s) + Au(s) + H_2(g) \rightarrow CsAuH_2$	−25.5	[d]		
$ {}^1/_3Cs_2Au_3(s)$[c] $ + {}^1/_3CsH(s) + {}^5/_6H_2(g) \rightarrow CsAuH_2$	−12.4	[d]		
$CsAu(s) + H_2(g) \rightarrow CsAuH_2$	−10.6	[d]		

[a]All possibilities are illustrated by the phase diagrams shown in Figure 5. The first lines provide corresponding calculated energies/heats of formation. Energies are given in kcal/mol for the reaction as written. Structures of alkali-gold binaries are taken from the Inorganic Crystal Structure Database (ICSD), unless otherwise specified. [b]The K_2Au composition is experimentally unknown. The *I*4/*mcm* structure used is the experimentally known ground state of Na_2Au. This phase does not necessarily correspond to the ground state of K_2Au, as our structure search revealed several other phases of similar energy. Because K_2Au is not directly relevant for the stability of $KAuH_2$, the exact structure matters less. [c]The Cs_2Au_3 composition is experimentally unknown. The *Immm* structure was here taken from the experimental K and Rb analogues. [d]Phonon calculations of the $CsAuH_2$ *C*2 phase revealed an imaginary mode. However, subsequent optimizations following the mode (without symmetry) failed to identify a minimum of lower energy. Because these calculations are intensive and expensive, and the exact identity of the ground state will not change our conclusions, we have chosen to focus our analysis on the $KAuH_2$ salt.

Concerns for Synthesis. While we are certain of the thermodynamic stability of $[A \geq K]AuH_2$ in the ground state, $T \rightarrow 0$ K, the situation changes at higher temperatures. Assuming a 1 atm standard state for $H_2(g)$, the formation of $KAuH_2$ is calculated to be favored by ∼0.7 kcal/mol at 300 K. The obvious entropic advantage of free H_2 works against $[A]AuH_2$ stability at elevated temperatures, which are likely required for synthesis. An elevated pressure of H_2 would be needed to compensate for the entropy increase associated with raising the temperature, and allow for synthesis.

Properties. The band gaps of stable alkali metal gold hydride ground states (A = K or a larger alkali metal) are predicted to be large. The band gaps of the *C*2 phases of $KAuH_2$ and $CsAuH_2$ calculate as 2.4 and 3.0 eV, respectively. These values were computed with the PBE functional, which is known to underestimate band gaps. Therefore, we can safely conclude that when made, these materials will be insulating under ambient conditions. The result is not surprising; these materials could be simply viewed as ionic compounds of closed shell A^+ ions and the equally closed shell AuH_2^- molecule.

The favored orientation of the AuH_2^- subunits in the *C*2 phase, shown in Figure 4, effectively hinders extended Au−Au overlap (mainly through d and p; see Figure 6), the mechanism by which these materials might narrow their band gap. However, such overlap is present in higher energy metastable phases. For example, the $P2_12_12_1$ and *I*4/*mcm* phases shown in Figure 3 have markedly smaller PBE band gaps of 1.2 and 1.1 eV, respectively. The band gap for the $P2_12_12_1$ phase (which has the smallest unit cell) was calculated with the more accurate hybrid exchange-correlation density functional HSE06, which provides a band gap estimate of 1.9 eV, i.e., 0.7 eV larger than that with PBE. The material is still likely to be semiconducting.

Figures 6 and 7 show the band structure, the density of states (DOS), and the phonon spectrum for the $P2_12_12_1$ phase of $KAuH_2$ at $P = 1$ atm. Note the strong Au−H mixing in the flat bands at −6 eV, and the partitioning of phonons into high frequency, mainly H, motions and low frequency, K and Au, vibrations. The narrow phonon bands point to molecular entities; in fact, the narrow bands develop around the molecular vibrational frequencies given in parentheses in Figure 7. In the band structure, we see mainly gold 5d orbitals in the region 0−3 eV below the Fermi level, with some Au 6s and 6p throughout. There is clearly Au−H bonding both in the lower, predominantly H bands at −6 eV and in the mainly Au 5d band. This is corroborated by a crystal orbital Hamilton population (COHP) analysis, as shown in the SI.

Seeking Metallicity: The Effect of Pressure on $KAuH_2$. Having established the stability of $[A \geq K]AuH_2$ at 1 atm, and their semiconducting/insulating electronic structures, we return to the application of pressure to modulate the material properties of these ternary hydrides. We focus on $KAuH_2$, whose predicted phase behavior at $P < 120$ GPa is shown in

DOI: 10.1021/jacs.7b04456
J. Am. Chem. Soc. 2017, 139, 8740−8751

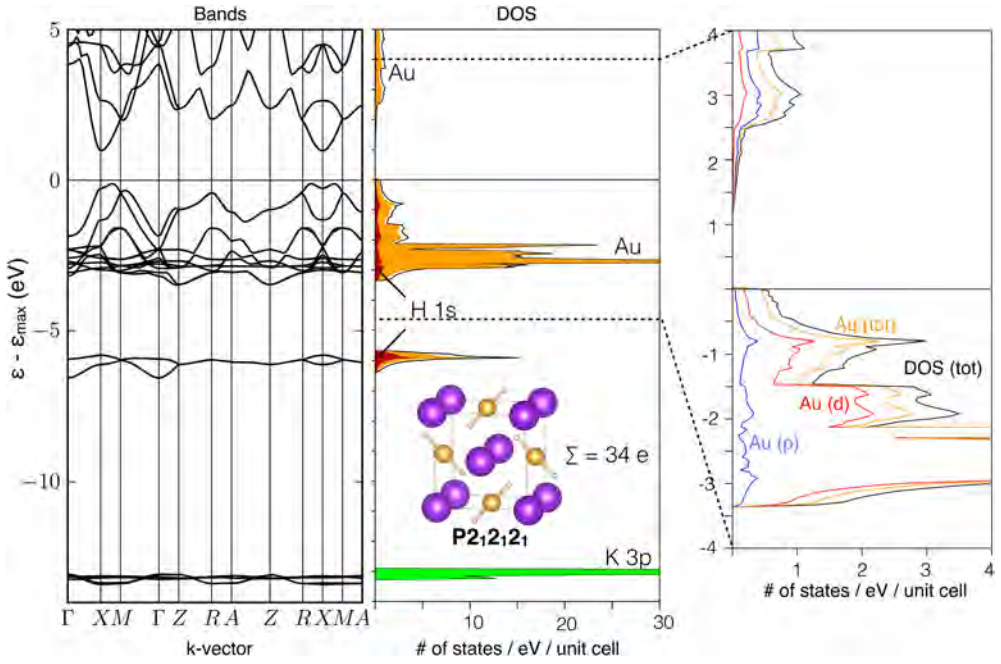

Figure 6. Band structure (left) and DOS (middle) of $KAuH_2$ in the metastable phase $P2_12_12_1$. Right inset shows the density of states close to the Fermi level, projected onto the 5d and 6p levels of gold; Au 5d-levels contribute mostly, with an admixture of Au 6p (and with H 1s as shown in the middle figure). There is a very small contribution from K 4p and 3d levels, trailing to zero at the Fermi level (not shown). The Au 6s-levels (projection not shown) are stabilized by interaction with H 1s (shown in red) and mirror the energy and dispersion of the latter closely.

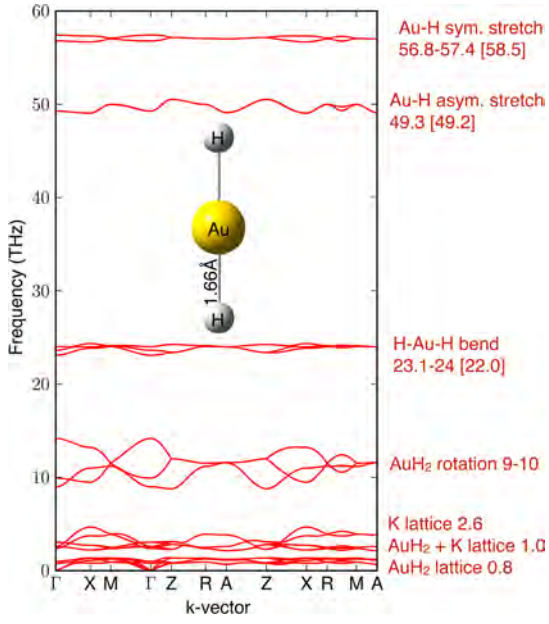

Figure 7. Phonon spectrum of $KAuH_2$ in the metastable phase $P2_12_12_1$. Assignments and comparison with calculations of gas-phase AuH_2^- are shown at right. Molecular vibrational frequencies are within brackets (1 THz ≡ 33.3 cm^{-1}). Model shows geometry of AuH_2^-, which is near identical when calculated in the gas phase and in the $KAuH_2$ crystal at 1 atm.

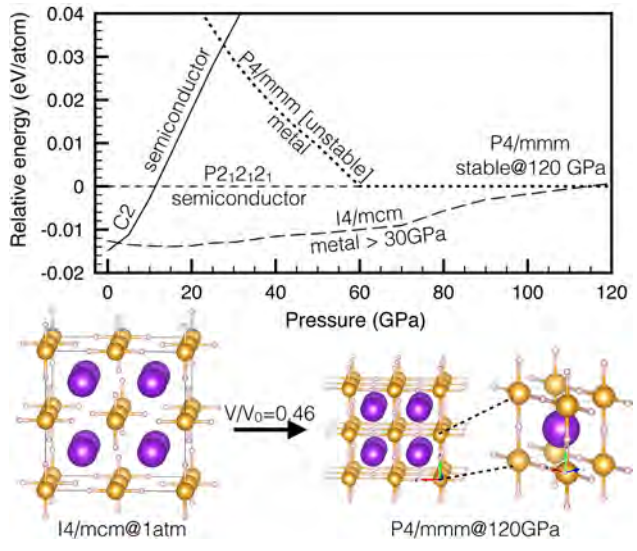

Figure 8. Competing phases of $KAuH_2$ under compression. The *C*2 phase is predicted to convert into *I*4/*mcm* at a couple of GPa. *I*4/*mcm* turns metallic at ∼30 GPa, and transforms into the Au−H−Au equidistant *P*4/*mmm* phase at ∼120 GPa. Structures at the bottom illustrate how the larger *I*4/*mcm* unit cell is related to the smaller *P*4/*mmm* unit cell. At a compression ratio of V/V_0 = 0.46, the *I*4/*mcm* structure acquires equidistant Au−H−Au bonds, and de facto equates to a 2 × 2 × 2 supercell of the smaller *P*4/*mmm* conventional cell.

Figure 8. For this system, the application of pressure acts to raise the crystal symmetry. The *C*2 phase quickly becomes less stable than a semiconducting *I*4/*mcm* phase at ∼2 GPa. The *I*4/*mcm* phase becomes metallic (at the PBE level) at ∼30 GPa, and converts into a *P*4/*mmm* phase at ∼120 GPa. The metastable $P2_12_12_1$ phase is predicted to convert into the same *P*4/*mmm* phase at 60 GPa.

The *I*4/*mcm* → *P*4/*mmm* phase transformation, predicted just before 120 GPa, is geometrically interesting; it positions the hydrogens equidistant (1.73 Å) from their neighboring Au atoms. This equates to the formation of square planar sheets of hydrogen atoms, bonded with square planar sheets of gold. The sheets are then stacked with K^+ ions. One sees here a structural relationship to cuprate sheets in the superconducting cuprates,[63] and to the $Im\bar{3}m$ SH_3 structure.[64] However, the

DOI: 10.1021/jacs.7b04456
J. Am. Chem. Soc. 2017, 139, 8740−8751

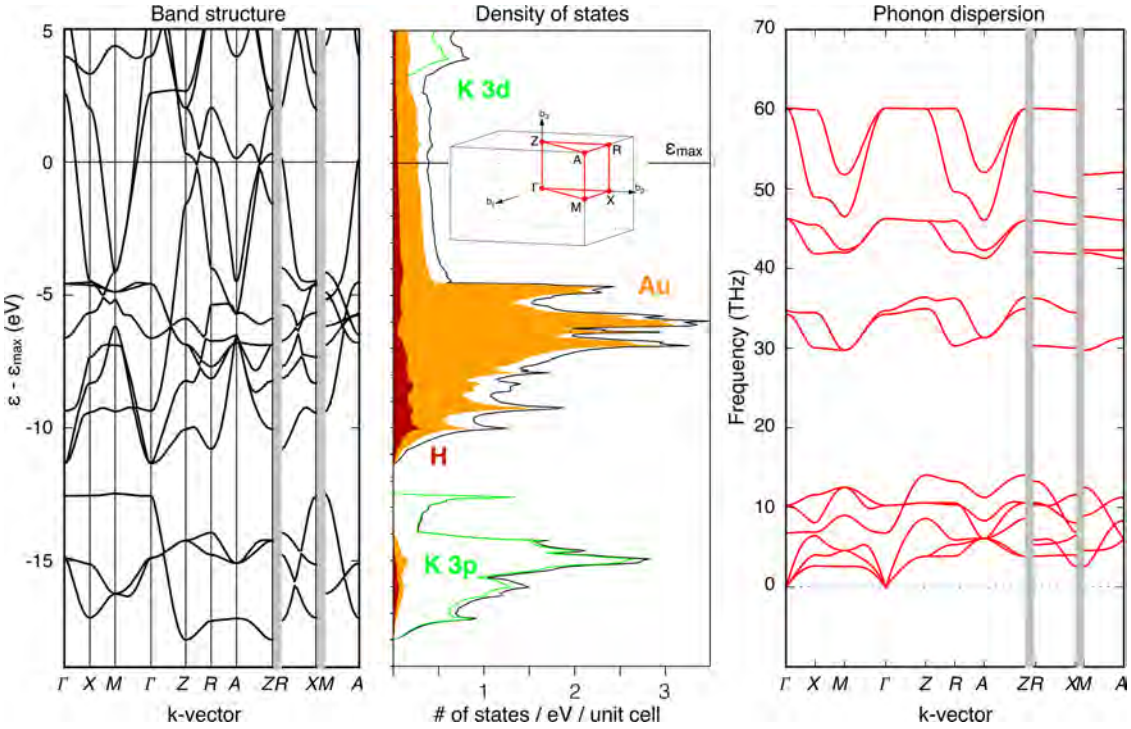

Figure 9. Band structure, density of states, and phonon spectrum (1 THz ≡ 33.3 cm^{-1}) of the Au−H−Au equidistant *P*4/*mmm* phase of $KAuH_2$ at 120 GPa. Inset in the middle figure shows the Brillouin zone path.

latter case has hydrogen bonding the sheets (there SH_2) together in a still more symmetrical ReO_3-type lattice.

The bands we see at *P* = 120 GPa (Figure 9) are, of course, broader than those we have previously shown in Figure 6. The Au 5d peak in the DOS is prominent in the region of −5 to −10 eV. Interestingly, even K 3p, formally a core level included in our calculation, acquires some dispersion at this pressure, around 10 eV. The density of states at the Fermi level is predominantly made up of formal Au d > p > s orbital contributions with an admixture of H 1s. The Au 6s, normally high in energy, is stabilized by interactions with H 1s. The population of Au 6p at the Fermi level can similarly be inferred from the frontier σ_u orbital of AuH_2^- spreading out into a band (see SI for orbitals of AuH_2^-). A comparison with pure gold, where the s-state contribution is very broad, penetrating into the d-block, is to be found in the SI.

We have not performed the search for the ground state of each Au−K binary under elevated pressures, a procedure required to ascertain the absolute phase stability of the *P*4/*mmm* with respect to decomposition. We nonetheless expect that the *P*4/*mmm* phase should be accessible experimentally (be it stable or metastable) by applying pressure to a sample of $KAuH_2$ obtained at 1 atm. The reasons for this are as follows: *C*2 is convertible into *I*4/*mcm* by following low frequency (~9 Thz ≡ 300 cm^{-1}) AuH_2^- rotational modes (Figure 7). No structural rearrangement occurs in the *I*4/*mcm* → *P*4/*mmm* transformation (Figure 8), which implies that the process is barrierless. The AuH_2^- anion is quite persistent in and of itself.[57]

In looking for pressure-induced metallicity, we have focused on $KAuH_2$ over $CsAuH_2$. This is because of $KAuH_2$'s predicted smaller band gap, and because Cs is too large to allow the formation of a corresponding high-pressure *P*4/*mmm* phase in which H is positioned equidistant between gold atoms. Next we show that a related strategy, of substituting alkali for alkaline earth metal ions, appears to provide a feasible route to metallic gold hydrides under ambient pressure conditions. The hunt for metallicity will lead us to tantalizing predictions of gold hydride-based superconductivity.

TERNARY ALKALINE EARTH METAL GOLD HYDRIDES

What happens if we substitute two alkali metal counterions by a single alkaline earth ion? One reason for looking at such compounds is to see the effect of cation size on the lattice stabilization and electronic structure, while comparing to the alkali metal ternaries where larger cations increased stability while also increasing band gaps. By concentrating the positive charge, we supposed that AuH_2^- subunits might be nudged closer, which should increase d-band dispersion and decrease band gaps. For the alkali metal ternaries we noticed that the radii[65] of the alkali metal cations follow the energy of formation linearly, which argues for even larger counterions still (see the SI). There are also additional reasons, related to theories of superconductivity, which will be addressed toward the end of this paper.

We searched for alkaline earth metal analogues, i.e. $[AE](AuH_2)_2$ stoichiometries (AE = Sr, Ba), while allowing for 1−3 formula units in each unit cell. The predicted ground states of $Sr(AuH_2)_2$ and $Ba(AuH_2)_2$ are of *I*4 symmetry. The ground state assignment of $Sr(AuH_2)_2$ is less certain, as our structure searches did identify one *I*4/*mcm* phase 1.5 kcal/mol lower than the *I*4 phase. However, the *I*4/*mcm* structure is not dynamically stable, and our attempts at making it so by lowering the crystal symmetry and following imaginary modes failed. For thermodynamic reasons that will be discussed, we will, however, focus mostly on $Ba(AuH_2)_2$. $Ba(AuH_2)_2$ is of *I*4 symmetry, and its predicted unit cell and structure at 1 atm is shown in Figure 10.

DOI: 10.1021/jacs.7b04456
J. Am. Chem. Soc. 2017, 139, 8740−8751

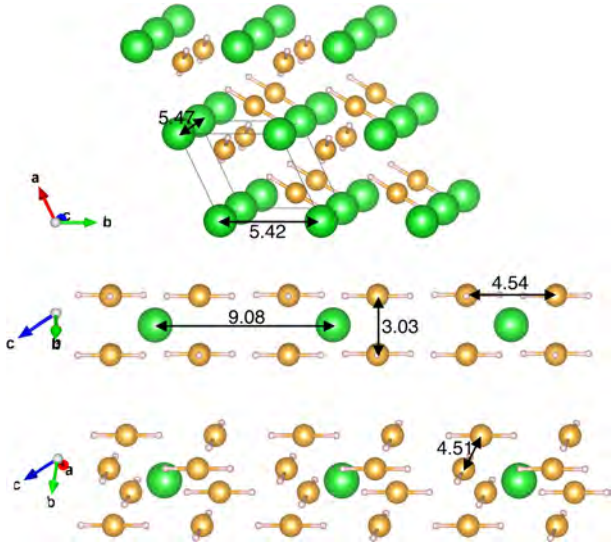

Figure 10. *I*4 structure of metastable $Ba(AuH_2)_2$ at 1 atm. Note how the AuH_2^- subunits arrange in a manner similar to what we found for the alkali metal analogues, but how voids are unavoidably introduced by replacing two singly charged alkali metal cations with one doubly charged Ba^{2+} cation.

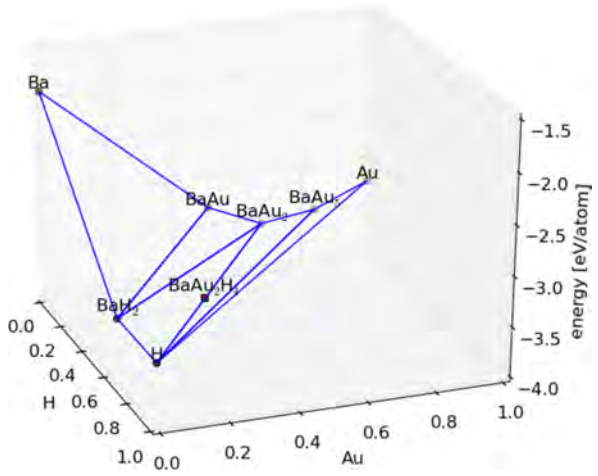

Figure 11. Calculated segment of the three-component phase diagram of Ba, Au, and H in the ground state (left). Blue lines between green circles connect stable phases. Unstable Au_xH_y binaries have been omitted. $Ba(AuH_2)_2$ is metastable (but just barely) with respect to decomposition into $BaAu_2$ and H_2. Its synthesis nevertheless appears possible from $CsAuH_2$.

Most of the ternary structures considered have nearest Au−Au separations far below the sum of the VdW distances (4−5 Å, depending on the formal oxidation state of gold). In the *C*2 and $P2_12_12_1$ phases of $KAuH_2$, for example, the nearest Au−Au distances are 3.94 and 3.77 Å, respectively. Could there be an aurophilic interaction at work here?[66−69] Since the phases of $KAuH_2$ that have longer and fewer Au−Au contacts are lower in energy (Figure 3) aurophilic bonding appears unlikely. This is a contrast to $Ba(AuH_2)_2$ where our suggested ground state exhibits a Au−Au distance of only 3.03 Å along one direction of the crystalline lattice (Figure 10).

Stability and Suggestions on Synthesis. The energy of formation (relative to AE(s), Au(s), and H_2(g)) of $Sr(AuH_2)_2$ and $Ba(AuH_2)_2$ are computed as −46 and −48 kcal/mol, respectively. These values are larger than the stabilization energies of the previously considered alkali salts (Table 1), in part a consequence of the larger formula unit. At the PBE level these phases are only metastable with respect to decomposition into $SrAu_2 + 2H_2$ (−5.2 kcal/mol) and $BaAu_2 + 2H_2$ (−4.0 kcal/mol), respectively. A piece of the 3D convex hull of the Ba/H/Au system is illustrated in Figure 11. The Sr/H/Au convex hull is shown in the SI.

However, as we have learned from our study of $KAuH_2$, PBE appears to slightly underestimate the stability of the ternary gold hydrides. Indeed, at the HSE06 level $Ba(AuH_2)_2$ *is* stable, ever so slightly, with respect to the most favored decomposition route:

$$Ba(AuH_2)_2 \rightarrow BaAu_2 + 2H_2, \quad \Delta E = +0.8 \text{ kcal/mol} \tag{1}$$

Note, however, that such a small endoergic reaction energy is not sufficient to counteract the favorable entropy increase associated with H_2 release. At the end of the day $Ba(AuH_2)_2$ is metastable, but just barely so. Fortunately, the large predicted kinetic stability of the AuH_2^- anion[57] suggests that metastability is no hindrance to synthesis of $Ba(AuH_2)_2$ or $Sr(AuH_2)_2$. Provided that $CsAuH_2$ is first made, and we think it can be, $Ba(AuH_2)_2$ and $Sr(AuH_2)_2$ should then be quite accessible via suitably chosen metathesis reactions, such as

$$2CsAuH_2 + BaBr_2 \rightarrow 2CsBr + Ba(AuH_2)_2, \quad \Delta E = -10 \text{ kcal/mol} \tag{2}$$

and

$$2CsAuH_2 + SrBr_2 \rightarrow 2CsBr + Sr(AuH_2)_2, \quad \Delta E = -13 \text{ kcal/mol} \tag{3}$$

Electronic Structures of $Sr(AuH_2)_2$ and $Ba(AuH_2)_2$. What about the electronic structures of $Ba(AuH_2)_2$ and $Sr(AuH_2)_2$? The band structure and density of states with orbital contributions of $Ba(AuH_2)_2$ are shown in Figure 12. The corresponding data for $Sr(AuH_2)_2$ and phonon band structures for both compounds are reproduced in the SI. The smaller size of the Ba-counterion (Table S2), compared to two alkali metal ions, requires the gold atoms to move closer. This has significant implications for the electronic structure. Especially one d-band of gold achieves a remarkable dispersion (Figure 12), which cross the Fermi level close to the zone center, then drops over 3 eV. A COHP analysis of the chemical bonding reveals largely concurrent Ba−H, Au−H, and Au−Au bonding below −2 eV and a weak antibonding contribution near −1 eV below the Fermi level.

In contrast to all alkali metal gold hydride phases explored, our PBE calculations suggest that $Ba(AuH_2)_2$ is metallic under ambient conditions. The density of states at the Fermi level is small, however, and it is possible that a lower energy structure, not identified by our structure search, may open up a gap. The shape of the density of states around the Fermi level is vaguely reminiscent to the DOS of graphene. Two prominent van Hove singularities are seen at −1 and −2.5 eV. Optimization at the HSE06 level of theory does not change the geometry in any meaningful way. However, HSE06 band structure calculations on $Ba(AuH_2)_2$ lead to an indirect gap (Γ → M) of ∼80 meV. Such a minuscule gap should close with thermal excitation even at low temperatures, and disappear with very mild shrinkage of the unit cell under compression. We have not included any

DOI: 10.1021/jacs.7b04456
J. Am. Chem. Soc. 2017, 139, 8740−8751

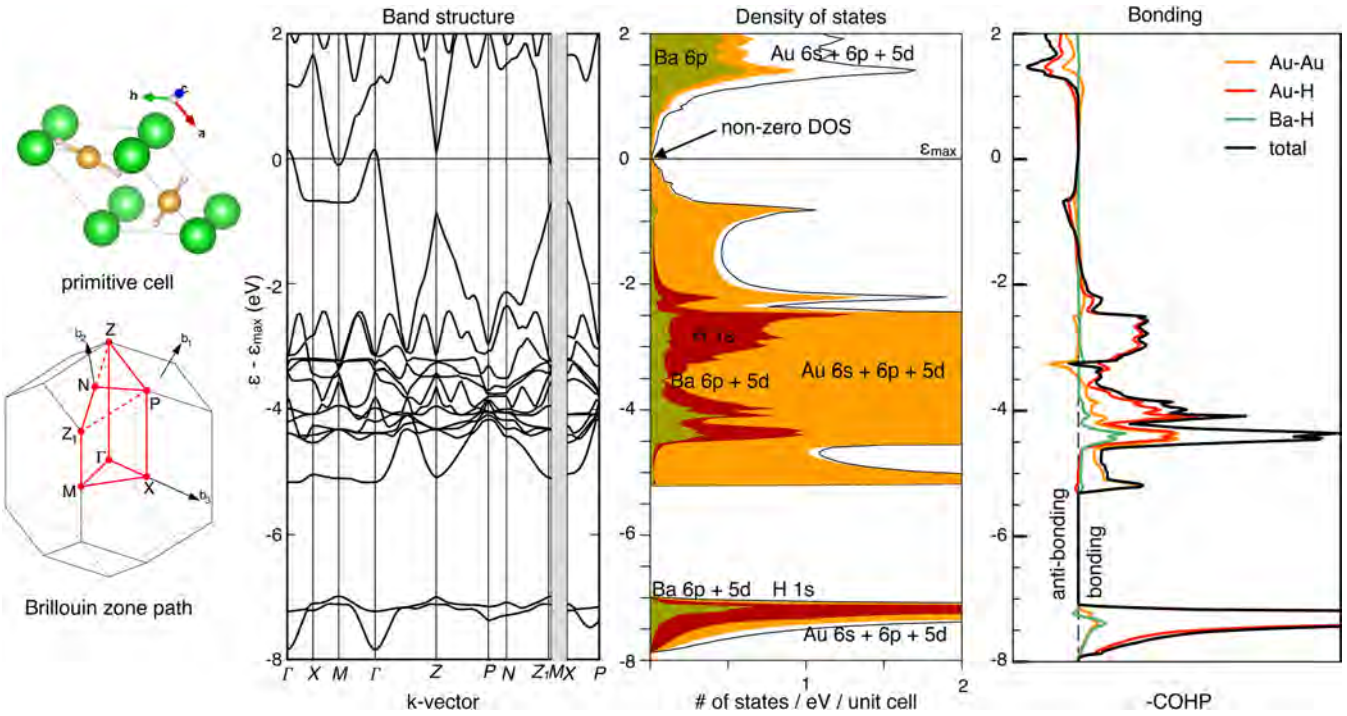

Figure 12. Unit cell, PBE band structure, and density of states (black line shows total) for $Ba(AuH_2)_2$ at 1 atm. Chemical bonding contributions are indicated by the Crystal Orbital Hamilton Population (COHP) at right.

correction for dispersion when obtaining the structures. This is because dispersion-uncorrected PBE provided unit cell volumes in better agreement with experimental reference data available for Li_2PdH_2 and Na_2PdH_2, which, however, arguably are subjected to thermal expansion (see the SI). With this in mind we are, if anything, overestimating the unit cell volumes. This sensitivity is important to keep in mind in later estimates of the electron phonon coupling, carried out at the PBE level.

The corresponding *I*4 phase of $Sr(AuH_2)_2$ is metallic at both levels of theory. The main difference between the band structure of $Sr(AuH_2)_2$ (shown in the SI) and that of $Ba(AuH_2)_2$, shown in Figure 12, is that the band just above the Fermi level at the Z-point in $Ba(AuH_2)_2$ crosses the Fermi level in $Sr(AuH_2)_2$.

Though not unprecedented at low pressures,[40−42] systems that are both ionic and metallic are not that common. Note the Ba 6p/5d−H 1s resonances in Figure 12. This is a sign of Ba−H bonding, not only Au−H. Such bonding needs to be considered for all compressed hydride structures. Ba−H bonding is also implied by the range of nearest-neighbor Ba−H bond distances of 3.17−2.87 Å, which are quite close to the 3.01−2.61 Å range in the *Pnma* ground state of BaH_2. A combined view, where the Ba−H sublattice is shown as prisms interlocked with AuH_2-bridges is shown in Figure 13.

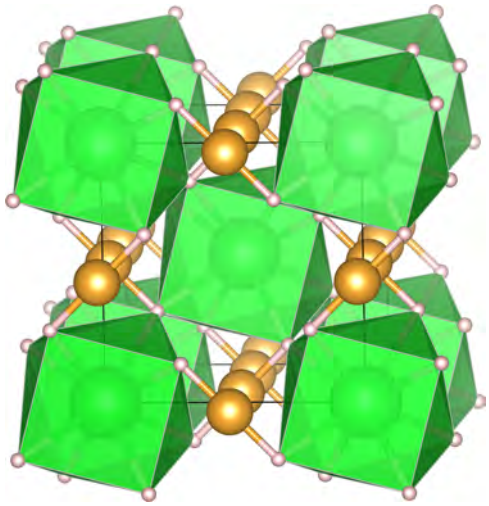

Figure 13. Conventional cell of $Ba(AuH_2)_2$ at 1 atm. The Ba−H sublattice is highlighted as green prisms centered with Ba ions.

THE MAKING OF A GOLD-HYDRIDE-BASED SUPERCONDUCTOR

One reason for looking into gold hydrides in the first place, aside from our academic interest in mitigating their nonexistence, is to search for novel superconducting materials. That hydrogen under high compression might form a phonon-mediated near room-temperature superconductor was proposed by one of us some time ago.[1] The realization that compression of alloys of hydrogen may allow for superconductivity at more moderate compressions[3] have since resulted in a flurry of theoretical and experimental work.[29]

Gold is *not* a superconducting element in its natural state,[70,71] but shows mK and μK superconductivity in alloys with Ga, Al, In, and Sn.[72,73] Whereas there are a few examples to the contrary (such as T_c = 1.5 K in $SrAuSi_3$[74]), superconductivity in gold compounds is rare. One proposed explanation is the avoidance of a +II oxidation state, and fluctuations around that as one sees in the cuprates.[75] However, Au^- is isoelectronic with Hg, which exhibits a critical superconducting temperature, T_c, of 4.2 K. If we limit our discussion to conventional superconductivity, then the most likely Cooper pairing mechanism (by popular consensus) is phonon-mediated. Au is, along with Cs and Ba, heavy, which

DOI: 10.1021/jacs.7b04456
J. Am. Chem. Soc. 2017, 139, 8740−8751

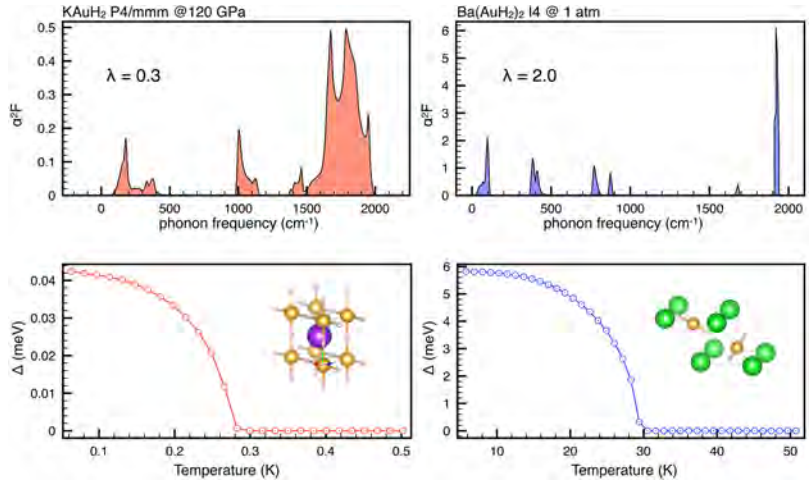

Figure 14. Top: Eliashberg spectral function, α^2F, for the $P4/mmm$ phase of $KAuH_2$ at 120 GPa and the $I4$ phase of $Ba(AuH_2)_2$ at 1 atm. Bottom: Superconducting gap as a function of temperature. Note the order(s) of magnitude difference in scale in λ, Δ, and T_c between the two materials.

lowers the frequency of soft lattice phonons. Low frequency phonon modes are important for increasing the electron phonon coupling constant, λ,

$$\lambda = 2\int \frac{\alpha^2F(\omega)}{\omega}\mathrm{d}\omega, \tag{4}$$

where α^2F is the Eliashberg spectral function, the phonon density of states weighted by an electron phonon coupling matrix element at each k-point and frequency. Whereas low phonon modes are important for raising λ, in turn crucial for a high T_c, they also decrease the average logarithmic frequency, ω_{log},

$$\omega_{log} = \exp\left[\frac{2}{\lambda}\int \alpha^2F(\omega)\frac{\ln(\omega)}{\omega}\mathrm{d}\omega\right]. \tag{5}$$

A reasonably high average frequency is another prerequisite for enabling higher T_c. So a balance has to be struck in the "design" of superconductive materials. The introduction of strong Au−H bonding, forming AuH_2^-, adds high frequency modes that increase ω_{log} dramatically. Together, λ and ω_{log} are key factors to consider for rationalizing the occurrence of superconductivity. One way to do so is through the McMillan-Allen-Dynes[2,76] approximation to the Eliashberg equations,[77,78]

$$T_c = \frac{\omega_{log}}{1.2}\exp\left[-\frac{1.04(1+\lambda)}{\lambda - \mu^*(1+0.62\lambda)}\right], \tag{6}$$

where μ^* is the electron-repulsion parameter, which typically is taken empirically to lie in the range of 0.10−0.15.

In addition to these arguments arising from traditional phonon-mediated superconductivity theory, there are other proposed Cooper pair formation mechanisms to consider. Purely electronic coupling via polaron and bipolarons[79] and polarization waves arising in a localized core−electron framework[80] are two such suggestions. Even as they are difficult to implement in current electronic structure codes, the latter two suggest an importance of polarizability. Heavy elements are more polarizable, and few more so than Cs and Ba.[81]

The arguments for superconductivity in ternary gold hydrides are enticing. However, a prerequisite is a metallic ground state. We have discussed two gold-hydride compounds in more detail, $KAuH_2$ under high compression, and $Ba(AuH_2)_2$ at 1 atm. How do they fare with respect to superconductivity?

The high-pressure $P4/mmm$ phase of $KAuH_2$ is predicted to be a superconductor, albeit with a quite meager T_c of 0.3 K at 120 GPa. The electron−phonon coupling constant λ calculates as 0.3, which places this material within the weak-coupling limit where the McMillan−Allen−Dynes approximation works well. The T_c of 0.3 K was calculated using a Coulomb pseudopotential parameter μ^* set to 0.11. We single out this value of μ^* as it also reproduces the T_c obtained after iteratively solving the Eliashberg equations (Figure 14).

The electron−phonon coupling λ is, in the limit of homogeneous coupling in k-space, proportional to the density of states at the Fermi level, $N(\varepsilon_F)$, which in the case of $KAuH_2$ at 120 GPa is dominated by Au-d states. From the flat density of states on both sides of the Fermi level (Figure 9) we can infer that no additional bands can be made to contribute to $N(\varepsilon_F)$, and that little can be gained, in terms of λ, from further compression of $KAuH_2$ beyond 120 GPa.

Turning then to $Ba(AuH_2)_2$ at 1 atm, our calculations predict a T_c of ∼30 K. This analysis hinges on its poor metallicity, a property, as we described, of which we cannot be completely certain. The Fermi surface is limited, with pockets of holes only close to the Γ-point, and of electrons near M in the Brillouin zone. Sensitivity of the electronic structure with respect to lattice distortion (phonon motion and the unit cell volume) is suggested both by the band structure near Γ and when comparing the M and Z points, where the latter shows an unfilled conduction band very close to the Fermi level. At our level of theory, the electron phonon coupling comes out as λ = 2.0. This is unusually large and comparable to DFT estimates of λ = 1.5−2.5 in high-pressure H_3S,[82−85] the phase believed responsible for T_c = 203 K superconductivity in compressed H_2S.[86]

The strong coupling predicted for $Ba(AuH_2)_2$ limits the reliability of the McMillan−Allen−Dynes approximation (eq 6). Nevertheless, when μ^* = 0.12 is chosen, eq 6 provides a T_c in good agreement with the numerical solution to the Eliashberg equations, which predict superconducting gap closure at ∼30 K (Figure 14). In comparison, the $I4$ phase of $Sr(AuH_2)_2$ has a smaller calculated electron phonon coupling constant λ of 0.9, and is predicted to turn superconducting below 10 K.

DOI: 10.1021/jacs.7b04456
J. Am. Chem. Soc. 2017, 139, 8740−8751

CONCLUSIONS

This work begins by computationally showing the infeasibility of preparing simple binary gold hydrides at any pressure below 300 GPa. This is not a reason for giving up in a quest for stable hydrides of Au. Turning to ternary compounds, we consider the kinetically stable AuH_2^- anion and predict that it can be stabilized in the condensed phase under ambient conditions (P = 1 atm, T = 298 K) by the introduction of both alkali ($M_w \geq$ K) and alkaline earth (Ba and Sr) counterions.

Exploration of ternary phase diagrams is never easy, but a careful analysis indicates that the AuH_2 salts of K, Rb and Cs are all thermodynamically stable. It should be possible to synthesize them from the elements under an excess of H_2. $CsAuH_2$ is the most stable ternary and, in turn, the most promising intermediate for the formation of metastable $Ba(AuH_2)_2$ and $Sr(AuH_2)_2$ via suitably chosen metathesis reactions. The thermodynamics discussed, and the inherent stability of AuH_2^- in isolation, makes us optimistic as to the possibility of high barriers to decomposition of $[A]AuH_2$ and $[AE](AuH_2)_2$ and the possibility of room temperature handling.

The alkali salts are semiconducting, with band gaps in the range of 2−3 eV. In looking for ways to attain metallicity in such compounds, we have done a more detailed analysis of the smallest band gap semiconductor that is predicted stable, namely, $KAuH_2$. The computed ionic ground state is made up of well-separated AuH_2^- molecular subunits; the predominant molecular character is clear from the limited phonon dispersion, which mirrors closely the vibrational frequencies of the isolated molecular anion. Upon compression, $KAuH_2$ is predicted to metallize at ∼30 GPa, and at ∼120 GPa, to lose all molecular character and transform into a Au−H−Au equidistant network, square sheets sandwiching a K^+ layer. The high pressure $KAuH_2$ structure is predicted to have a superconducting critical temperature of 0.3 K.

A metallic state is facilitated by Au-d level overlap. To enable this under ambient conditions we replace alkali metal counterions with barium and strontium, which necessitates AuH_2^- units moving closer together. The molecular, ionic, barely metallic solid $Ba(AuH_2)_2$ has a small Fermi surface, which makes electron−phonon coupling calculations sensitive to the level of theory, meriting caution and further study. With that disclaimer, we predict $Ba(AuH_2)_2$ to be a superconductor below 30 K at P = 1 atm. The analogous phase of $Sr(AuH_2)_2$ is calculated to be a superconductor below 10 K.

More importantly than the final predicted T_c is the route we took there, which sets out some design principles. Starting with light and heavy atoms (suggested by a phonon mediated BCS view of superconductivity) we overcame an electronic hindrance to phase stability by moving from a binary to a ternary, incorporating alkali metal ions. This is a chemical maneuver rooted in electronegativity considerations. A second instance of chemical reasoning, essentially steric or ion size considerations, led us from $KAuH_2$ semiconducting (at P = 1 atm) to borderline metallic and computed as superconducting $Ba(AuH_2)_2$ and $Sr(AuH_2)_2$. Throughout we paid attention to realistic prospects of synthesis. We believe we have opened up new "search spaces" for superconductivity, and have made good use of chemical ideas in devising strategies for attaining new superconductors.

METHODOLOGY

Geometry Optimization. Initial calculations relied on periodic DFT calculations performed using VASP, version 5.3.5.[87,88] The Predew−Burke−Ernzerhof (PBE)[89] generalized gradient approximation (GGA) functional was used to generate electronic wave functions that were expanded in a plane-wave basis set with a kinetic energy cutoff of 800 eV. Projected augmented wave (PAW) potentials[88,90] were used to treat core electrons and incorporate the associated relativistic effects of gold. The number of explicitly treated electrons were $ns(n-1)p^6$ for alkali and alkaline earth metal atoms, $1s^1$ for H, and $6s^15d^9$ for Au. Brillouin zone sampling was performed on k-meshes with a reciprocal space resolution of at least $2\pi \times 0.03$ Å^{-1}. Energies and their gradients were converged to <1 meV per atom. This approach provided geometries in excellent agreement with experimental X-ray structures for the related Li_2PdH_2 and Na_2PdH_2 salts (see the SI), and this level of theory was therefore used throughout. Dispersion correction (DFT-D3) caused an underestimation (∼10%) of the unit cell volumes, and for this reason this correction was not used. We stress that this is not necessarily a fault of the DFT-D3 correction, but at least partly a consequence of us omitting the effects of thermal expansion in the materials when comparing to experimental data obtained at $T > 0$.

Electronic Structure. In addition to using PBE throughout, selected relative energies and densities of states were refined using the Heyd−Scuseria−Ernzerhof (HSE06)[91,92] screened-hybrid functional, using either a 400 or 600 eV kinetic energy cutoff. HSE06 has a reported mean absolute error of 0.2 eV for band gaps.[93] Compared to the more accurate HSE06 method, PBE was consistently found to underestimate the relative energy of discussed ternary systems, i.e., offer a more conservative estimate to their stability. The reasonably small differences (<4.5 kcal/mol) between HSE06 and PBE are of little consequence to our conclusions.

Structure Prediction. Searches for the global minima on the potential energy surface were performed using a particle swarm optimization algorithm[94] implemented in the CALYPSO code.[95] Typically two or more structure searches, each allowing for 1−4 units of a given stoichiometry, were performed. The reliability of the approach was validated on a related ternary system; the algorithm correctly identified the experimentally known $I4/mmm$ ground state of Li_2PdH_2 and Na_2PdH_2.

Dynamic Stability. Thermal corrections to the energies were calculated from force constants obtained through the direct method,[96] i.e., from Hellmann−Feynman forces induced by small displacements introduced to a supercell, using the PHONOPY 1.9.7 code.[97] For the phonon calculations a kinetic energy cutoff of 400 eV was used.

Superconductivity. The Full Potential Linear Augmented Plane Wave (FP-LAPW) method implemented in the ELK code[98] was used for calculating T_c using both eq 6, and by iteratively solving the Eliashberg equations. Initial muffin tin radii used were Ba_{1atm} = 2.4, Sr_{1atm} = 2.6, K_{120GPa} = 2.0, Au_{1atm} = 2.1, Au_{120GPa} = 1.8, H_{1atm} = 1.1, and H_{120GPa} = 1.2 bohr. Phonons were calculated using a supercell approach similar to what is described above, where for $KAuH_2$ and $[Ba/Sr](AuH_2)_2$ we used a 3 × 3 × 3 and 2 × 2 × 2 supercell, respectively. Electron−phonon coupling for the latter compounds was evaluated using 32 × 32 × 32 k-meshes. Convergence of the phonon density of states and Gibbs energy with respect to supercell size was made with VASP (see the SI). The inclusion

DOI: 10.1021/jacs.7b04456
J. Am. Chem. Soc. 2017, 139, 8740−8751

of spin−orbit coupling had very minor influences on the Fermi surface of compressed $KAuH_2$, and no effect on the Fermi surface of $Ba(AuH_2)_2$ (see the SI).

This work relied on the Atomic Simulation Environment (ASE)[99] and AFLOW.[100]

■ ASSOCIATED CONTENT

Supporting Information

The Supporting Information is available free of charge on the ACS Publications website at DOI: 10.1021/jacs.7b04456.

Comparisons with the experimental structures of Li_2PdH_2 and Na_2PdH_2; calculated convex hulls and vibrational analyses of selected materials; electronic structure analyses, including band structures, COHP analyses, orbital projections, and the effect of spin−orbit coupling in selected materials; calculated radii of some atoms, anions and cations, and their relation to the energy of formation of gold hydride ternaries; phonon convergence tests; optimized geometries of all structures in cif format (PDF)

■ AUTHOR INFORMATION

Corresponding Authors

*martin.rahm@chalmers.se
*rh34@cornell.edu

ORCID

Martin Rahm: 0000-0001-7645-5923
Roald Hoffmann: 0000-0001-5369-6046

Present Address

§M.R.: Department of Chemistry and Chemical Engineering, Physical Chemistry, Chalmers University of Technology, Gothenburg SE-412 96, Sweden.

Notes

The authors declare no competing financial interest.

■ ACKNOWLEDGMENTS

This work was supported by EFree, an Energy Frontier Research Center funded by the U.S. Department of Energy (DOE) Office of Science, Basic Energy Sciences (BES), under grant no. DE-SC0001057. Calculations presented in this work used the Extreme Science and Engineering Discovery Environment (XSEDE),[101] which is supported by NSF grant number ACI-1053575. This work was performed in part at the Cornell NanoScale Facility, a member of the National Nanotechnology Coordinated Infrastructure (NNCI), which is supported by the National Science Foundation (Grant ECCS-1542081)

■ REFERENCES

(1) Ashcroft, N. W. *Phys. Rev. Lett.* **1968**, *21*, 1748−1749.
(2) Allen, P. B.; Dynes, R. C. *Phys. Rev. B* **1975**, *12*, 905−922.
(3) Ashcroft, N. W. *Phys. Rev. Lett.* **2004**, *92*, 187002.
(4) Donnerer, C.; Scheler, T.; Gregoryanz, E. *J. Chem. Phys.* **2013**, *138*, 134507.
(5) Silverwood, I. P.; Rogers, S. M.; Callear, S. K.; Parker, S. F.; Catlow, C. R. A. *Chem. Commun. (Cambridge, U. K.)* **2016**, *52*, 533−536.
(6) Degtyareva, V. F. *J. Alloys Compd.* **2015**, *645*, S128−S131.
(7) Mudring, A.-V.; Jansen, M. *Angew. Chem., Int. Ed.* **2000**, *39*, 3066−3067.
(8) Feldmann, C.; Jansen, M. *Angew. Chem.* **1993**, *105*, 1107−8; See also *Angew. Chem., Int. Ed. Engl.* **1993**, *32* (7), 1049.
(9) Feldmann, C.; Jansen, M. *Z. Anorg. Allg. Chem.* **1995**, *621*, 201−206.
(10) Maya, L.; Paranthaman, M.; Thundat, T.; Bauer, M. L. *J. Vac. Sci. Technol., B: Microelectron. Process. Phenom.* **1996**, *14*, 15−21.
(11) Tsai, H.; Hu, E.; Perng, K.; Chen, M.; Wu, J.-C.; Chang, Y.-S. *Surf. Sci.* **2003**, *537*, L447−L450.
(12) Tchaplyguine, M.; Mikkelae, M.-H.; Zhang, C.; Andersson, T.; Bjoerneholm, O. *J. Phys. Chem. C* **2015**, *119*, 8937−8943.
(13) Hermann, A.; Derzsi, M.; Grochala, W.; Hoffmann, R. *Inorg. Chem.* **2016**, *55*, 1278−1286.
(14) Ringström, U. *Nature* **1963**, *198*, 981.
(15) Wang, X.; Andrews, L. *J. Am. Chem. Soc.* **2001**, *123*, 12899−12900.
(16) Wang, X.; Andrews, L. *J. Phys. Chem. A* **2002**, *106*, 3744−3748.
(17) Dulong, P. L.; Thenard, L. G. *Ann. Chim. Phys.* **1823**, *23*, 440.
(18) Dulong, P. L.; Thenard, L. G. *Ann. Chim. Phys.* **1823**, *24*, 380.
(19) Haruta, M.; Kobayashi, T.; Sano, H.; Yamada, N. *Chem. Lett.* **1987**, *16*, 405−408.
(20) Miao, M.-S.; Kurzman, J. A.; Mammen, N.; Narasimhan, S.; Seshadri, R. *Inorg. Chem.* **2012**, *51*, 7569−7578.
(21) Lehner, H.; Matt, D.; Pregosin, P. S.; Venanzi, L. M.; Albinati, A. *J. Am. Chem. Soc.* **1982**, *104*, 6825−6827.
(22) Jordan, A. J.; Lalic, G.; Sadighi, J. P. *Chem. Rev. (Washington, DC, U. S.)* **2016**, *116*, 8318−8372.
(23) Tsui, E. Y.; Muller, P.; Sadighi, J. P. *Angew. Chem., Int. Ed.* **2008**, *47*, 8937−8940.
(24) Escalle, A.; Mora, G.; Gagosz, F.; Mezailles, N.; Le Goff, X. F.; Jean, Y.; Le Floch, P. *Inorg. Chem.* **2009**, *48*, 8415−8422.
(25) Rosca, D.-A.; Smith, D. A.; Hughes, D. L.; Bochmann, M. *Angew. Chem., Int. Ed.* **2012**, *51*, 10643−10646.
(26) Pintus, A.; Rocchigiani, L.; Fernandez-Cestau, J.; Bochmann, M.; Budzelaar, P. H. M. *Angew. Chem., Int. Ed.* **2016**, *55*, 12321−12324.
(27) Schmidbaur, H.; Raubenheimer, H. G.; Dobrzanska, L. *Chem. Soc. Rev.* **2014**, *43*, 345−380.
(28) Grochala, W.; Hoffmann, R.; Feng, J.; Ashcroft, N. W. *Angew. Chem., Int. Ed.* **2007**, *46*, 3620−3642.
(29) Zhang, L.; Wang, Y.; Lv, J.; Ma, Y. *Nat. Rev. Mater.* **2017**, *2*, 17005.
(30) Mann, J. B.; Meek, T. L.; Knight, E. T.; Capitani, J. F.; Allen, L. C. *J. Am. Chem. Soc.* **2000**, *122*, 5132−5137.
(31) Mann, J. B.; Meek, T. L.; Allen, L. C. *J. Am. Chem. Soc.* **2000**, *122*, 2780−2783.
(32) Barbaras, G. D.; Dillard, C.; Finholt, A. E.; Wartik, T.; Wilzbach, K. E.; Schlesinger, H. I. *J. Am. Chem. Soc.* **1951**, *73*, 4585−4590.
(33) Wang, X.; Andrews, L. *Phys. Chem. Chem. Phys.* **2005**, *7*, 750−759.
(34) Kadir, K.; Kritikos, M.; Noréus, D.; Andresen, A. F. *J. Less-Common Met.* **1991**, *172−174*, 36−41.
(35) Bronger, W.; Brassard, L. A. *Z. Anorg. Allg. Chem.* **1996**, *622*, 462−464.
(36) Bronger, W.; Auffermann, G. *Chem. Mater.* **1998**, *10*, 2723−2732.
(37) Bronger, W. *Angew. Chem.* **1991**, *103*, 776−84; See also *Angew. Chem., Int. Ed. Engl.* **1991**, *30* (7), 759.
(38) Noréus, D.; Törnroos, K. W.; Börje, A.; Szabo, T.; Bronger, W.; Spittank, H.; Auffermann, G.; Müller, P. *J. Less-Common Met.* **1988**, *139*, 233−239.
(39) Suchanek, E.; Lange, N.; Auffermann, G.; Bronger, W.; Lutz, H. D. *J. Raman Spectrosc.* **1999**, *30*, 981−986.
(40) Olofsson-Mårtensson, M.; Häussermann, U.; Tomkinson, J.; Noréus, D. *J. Am. Chem. Soc.* **2000**, *122*, 6960−6970.
(41) Orgaz, E.; Gupta, M. *J. Alloys Compd.* **1997**, *253−254*, 326−329.
(42) Orgaz, E.; Gupta, M. *Int. J. Quantum Chem.* **2000**, *80*, 141−152.
(43) Yvon, K. *Z. Kristallogr. - Cryst. Mater.* **2003**, *218*, 108−116.
(44) Schlapbach, L.; Zuettel, A. *Nature* **2001**, *414*, 353−358.
(45) Puhakainen, K.; Stoyanov, E.; Evans, M. J.; Leinenweber, K.; Häussermann, U. *J. Solid State Chem.* **2010**, *183*, 1785−1789.

DOI: 10.1021/jacs.7b04456
J. Am. Chem. Soc. 2017, 139, 8740−8751

(46) Nicholson, K. M.; Sholl, D. S. *Inorg. Chem.* **2014**, *53*, 11849−11860.
(47) Sommer, A. *Nature (London, U. K.)* **1943**, *152*, 215.
(48) Spicer, W. E.; Sommer, A. H.; White, J. G. *Phys. Rev.* **1959**, *115*, 57−62.
(49) Kienast, G.; Verma, J.; Klemm, W. *Z. Anorg. Allg. Chem.* **1961**, *310*, 143−169.
(50) Liu, T. L. *Phys. Rev. B* **1975**, *12*, 3008−3012.
(51) Tinelli, G. A.; Holcomb, D. F. *J. Solid State Chem.* **1978**, *25*, 157−168.
(52) Busse, B.; Weil, K. G. *Ber. Bunsenges. Phys. Chem.* **1981**, *85*, 309−313.
(53) Zachwieja, U. *Z. Anorg. Allg. Chem.* **1993**, *619*, 1095−1097.
(54) Grosch, G. H.; Range, K.-J. *J. Alloys Compd.* **1996**, *233*, 30−38.
(55) Miao, M.; Brgoch, J.; Krishnapriyan, A.; Goldman, A.; Kurzman, J. A.; Seshadri, R. *Inorg. Chem.* **2013**, *52*, 8183−8189.
(56) Wang, X.; Andrews, L. *Angew. Chem., Int. Ed.* **2003**, *42*, 5201−5206.
(57) Dorta-Urra, A.; Zanchet, A.; Roncero, O.; Aguado, A. *J. Chem. Phys.* **2015**, *142*, 154301.
(58) Zurek, E.; Hoffmann, R.; Ashcroft, N. W.; Oganov, A. R.; Lyakhov, A. O. *Proc. Natl. Acad. Sci. U. S. A.* **2009**, *106*, 17640−17643.
(59) Hooper, J.; Zurek, E. *J. Phys. Chem. C* **2012**, *116*, 13322−13328.
(60) Hooper, J.; Altintas, B.; Shamp, A.; Zurek, E. *J. Phys. Chem. C* **2013**, *117*, 2982−2992.
(61) Pickard, C. J.; Needs, R. J. *J. Phys.: Condens. Matter* **2011**, *23*, 053201.
(62) Jain, A.; Ong, S. P.; Hautier, G.; Chen, W.; Richards, W. D.; Dacek, S.; Cholia, S.; Gunter, D.; Skinner, D.; Ceder, G.; Persson, K. A. *APL Mater.* **2013**, *1*, 011002.
(63) Weller, M. T.; Knee, C. S. *J. Mater. Chem.* **2001**, *11*, 701−712.
(64) Duan, D.; Liu, Y.; Tian, F.; Li, D.; Huang, X.; Zhao, Z.; Yu, H.; Liu, B.; Tian, W.; Cui, T. *Sci. Rep.* **2015**, *4*, 6968.
(65) Rahm, M.; Hoffmann, R.; Ashcroft, N. W. *Chem. - Eur. J.* **2016**, *22*, 14625−14632.
(66) Scherbaum, F.; Grohmann, A.; Huber, B.; Krüger, C.; Schmidbaur, H. *Angew. Chem., Int. Ed. Engl.* **1988**, *27*, 1544−1546.
(67) Pyykkö, P. *Chem. Rev. (Washington, DC, U. S.)* **1997**, *97*, 597−636.
(68) Schmidbaur, H. *Gold Bull. (London)* **2000**, *33*, 3−10.
(69) Schmidbaur, H.; Schier, A. *Chem. Soc. Rev.* **2012**, *41*, 370−412.
(70) Ono, K.; Asahi, K.; Nishida, N.; Ray, J.; Ishimoto, H. *Physica B +C (Amsterdam)* **1981**, *107*, 719−720.
(71) Buchal, C.; Mueller, R. M.; Kubota, M.; Pobell, F. *Physica B+C (Amsterdam)* **1981**, *108*, 1331−1332.
(72) Hoyt, R. F.; Mota, A. C. *Solid State Commun.* **1976**, *18*, 139−142.
(73) Zadorozhny, Y.; Liu, Y. *Phys. Rev. B: Condens. Matter Mater. Phys.* **2002**, *66*, 054512.
(74) Isobe, M.; Yoshida, H.; Kimoto, K.; Arai, M.; Takayama-Muromachi, E. *Chem. Mater.* **2014**, *26*, 2155−2165.
(75) Larsson, S. *Chem. - Eur. J.* **2004**, *10*, 5276−5283.
(76) McMillan, W. L. *Phys. Rev.* **1968**, *167*, 331−344.
(77) Carbotte, J. P. *Rev. Mod. Phys.* **1990**, *62*, 1027−1157.
(78) Eliashberg, G. M. *Zh. Eksp. Teor. Fiz.* **1960**, *38*, 966−976.
(79) Alexandrov, A. S.; Mott, N. F. *Rep. Prog. Phys.* **1994**, *57*, 1197−1288 and references therein.
(80) Atwal, G. S.; Ashcroft, N. W. *Phys. Rev. B: Condens. Matter Mater. Phys.* **2004**, *70*, 104513.
(81) Schwerdtfeger, P. *At., Mol. Clusters Electr. Fields* **2006**, 1−32.
(82) Errea, I.; Calandra, M.; Pickard, C. J.; Nelson, J.; Needs, R. J.; Li, Y.; Liu, H.; Zhang, Y.; Ma, Y.; Mauri, F. *Phys. Rev. Lett.* **2015**, *114*, 157004.
(83) Papaconstantopoulos, D. A.; Klein, B. M.; Mehl, M. J.; Pickett, W. E. *Phys. Rev. B: Condens. Matter Mater. Phys.* **2015**, *91*, 184511.
(84) Komelj, M.; Krakauer, H. *Phys. Rev. B: Condens. Matter Mater. Phys.* **2015**, *92*, 205125.
(85) Flores-Livas, J.; Sanna, A.; Gross, E. K. U. *Eur. Phys. J. B* **2016**, *89*, 63.
(86) Drozdov, A. P.; Eremets, M. I.; Troyan, I. A.; Ksenofontov, V.; Shylin, S. I. *Nature (London, U. K.)* **2015**, *525*, 73−76.
(87) Kresse, G.; Furthmueller, J. *Phys. Rev. B: Condens. Matter Mater. Phys.* **1996**, *54*, 11169−11186.
(88) Kresse, G.; Joubert, D. *Phys. Rev. B: Condens. Matter Mater. Phys.* **1999**, *59*, 1758−1775.
(89) Perdew, J. P.; Burke, K.; Ernzerhof, M. *Phys. Rev. Lett.* **1996**, *77*, 3865−3868.
(90) Bloechl, P. E. *Phys. Rev. B: Condens. Matter Mater. Phys.* **1994**, *50*, 17953−17979.
(91) Heyd, J.; Scuseria, G. E.; Ernzerhof, M. *J. Chem. Phys.* **2003**, *118*, 8207−8215.
(92) Izmaylov, A. F.; Scuseria, G. E.; Frisch, M. J. *J. Chem. Phys.* **2006**, *125*, 104103.
(93) Heyd, J.; Scuseria, G. E. *J. Chem. Phys.* **2004**, *121*, 1187−1192.
(94) Wang, Y.; Lv, J.; Zhu, L.; Ma, Y. *Phys. Rev. B: Condens. Matter Mater. Phys.* **2010**, *82*, 094116.
(95) Wang, Y.; Lv, J.; Zhu, L.; Ma, Y. *Comput. Phys. Commun.* **2012**, *183*, 2063−2070.
(96) Parlinski, K.; Li, Z. Q.; Kawazoe, Y. *Phys. Rev. Lett.* **1997**, *78*, 4063−4066.
(97) Togo, A.; Tanaka, I. *Scr. Mater.* **2015**, *108*, 1−5.
(98) *ELK*, v. 4.015; 2016; http://elk.sourceforge.net/.
(99) Bahn, S. R.; Jacobsen, K. W. *Comput. Sci. Eng.* **2002**, *4*, 56−66.
(100) Curtarolo, S.; Setyawan, W.; Hart, G. L. W.; Jahnatek, M.; Chepulskii, R. V.; Taylor, R. H.; Wang, S.; Xue, J.; Yang, K.; Levy, O.; Mehl, M. J.; Stokes, H. T.; Demchenko, D. O.; Morgan, D. *Comput. Mater. Sci.* **2012**, *58*, 218−226.
(101) Towns, J.; Cockerill, T.; Dahan, M.; Foster, I.; Gaither, K.; Grimshaw, A.; Hazlewood, V.; Lathrop, S.; Lifka, D.; Peterson, G. D.; Roskies, R.; Scott, J. R.; Wilkens-Diehr, N. *Comput. Sci. Eng.* **2014**, *16*, 62−74.

DOI: 10.1021/jacs.7b04456
J. Am. Chem. Soc. 2017, 139, 8740−8751